Supporting Information

Impact of pH on Aqueous-Phase Phenol Hydrogenation Catalyzed by Carbon-Supported Pt and Rh

Nirala Singh,[†,‡] Mal-Soon Lee,[‡] Sneha A. Akhade,[‡] Guanhua Cheng,[‖] Donald M. Camaioni,[‡] Oliver Y. Gutiérrez,[‡] Vassiliki-Alexandra Glezakou,[‡] Roger Rousseau,[*,‡] Johannes A. Lercher[*,‡,‖] Charles T. Campbell[*,†]

†Department of Chemistry, University of Washington, Seattle, Washington 98105-1700, United States

‡Institute for Integrated Catalysis, Pacific Northwest National Laboratory, Richland, Washington 99354, United States

‖Department of Chemistry and Catalysis Research Center, Technische Univeristät München, D-85748 Garching, Germany

* **Corresponding Authors Email:** roger.rousseau@pnnl.gov, johannes.lercher@ch.tum.de, charliec@uw.edu

Catalytic hydrogenation of phenol over platinum

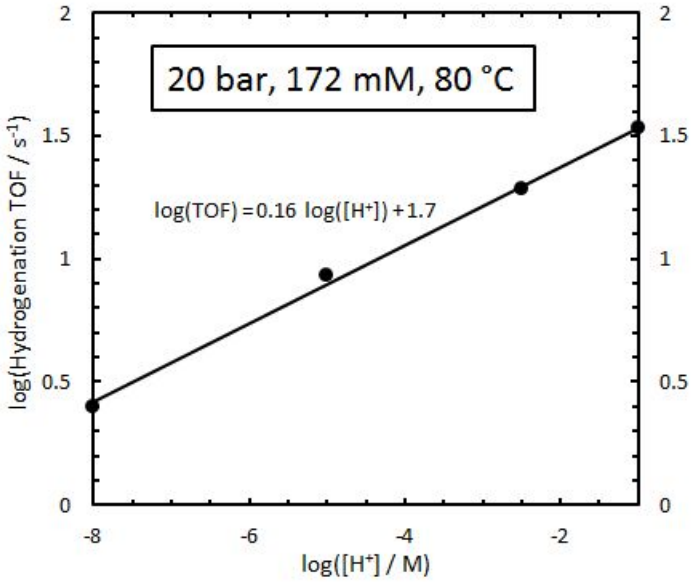

Figure S1. Log(TOF) for hydrogenation of phenol on 5 wt% Pt/C at 20 bar hydrogen, 172 mM phenol and 80 °C vs. log[H^+], showing the correlation of turnover frequency with proton concentration.

Table S1. Hydrogenation rates of phenol at different pH for 5 wt% Pt/C catalyst. Starting concentration of phenol is 18 mM in aqueous solution at room temperature, and 172 mM phenol at 80 °C. (This reaction is zero-order in phenol at both conditions.) The pH is adjusted using $HClO_4$, bicarbonate/carbonate or KOH. HBE are averaged from different electrolyte. *No detectable rate.

pH	HBE Pt(110) (kJ mol^{-1})[1]	Temp (°C)	Pressure (bar)	TOF (s^{-1})
1	-12.75	25	1	0.065
2.5	-12.9	25	1	0.092
5	-14.5	25	1	0.079
5	-14.5	25	1	0.065[2]
1	-12.75	80	20	34
2.5	-12.9	80	20	19
5	-14.5	80	20	8.5
8	-18.8	80	20	2.5
9.2	-20.0	80	20	0*

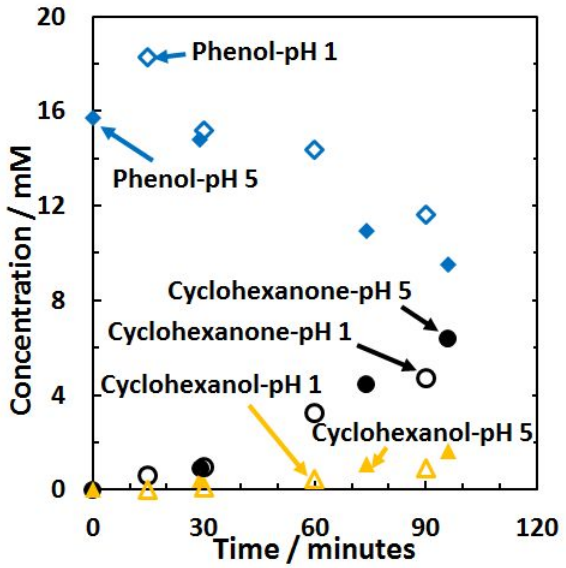

Figure S2. Concentrations of reactant and products as a function of time for 1 bar hydrogen pressure for pH 5 and pH 1 using 5 mg 5 wt% Pt/C catalyst at room temperature, starting with 18 mM phenol in water. Measurement at pH 5 is from [2]. The apparent difference in starting phenol concentration is due to variations in solution preparation and extraction efficiency (carbon balance >80%).

At 1 bar hydrogen and 25 °C, there is no observed change in the reaction rate or product distribution between pH 1 and pH 5 (Figure S2), unlike what is observed at 20 bar hydrogen and 80 °C.

Phenol hydrogenation over platinum compared to hydrogen evolution and oxidation

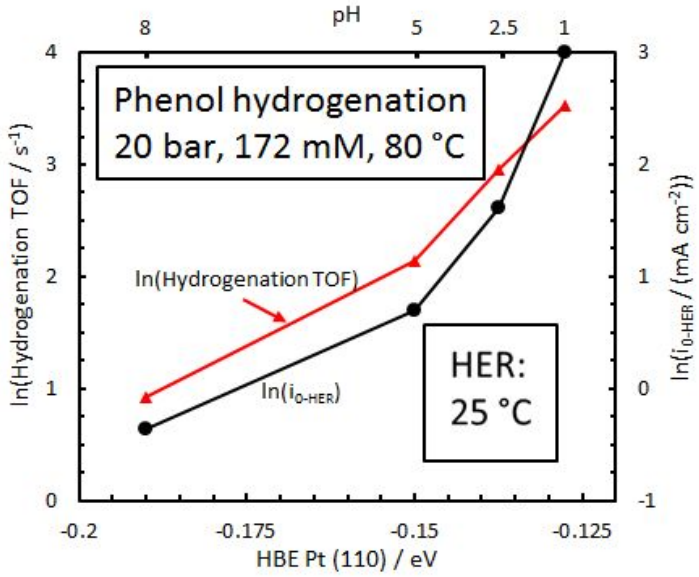

Figure S3. The pH dependence of the log(TOF) for hydrogenation of phenol at 80 °C for Pt/C and log ($i_{0\text{-HER}}$) for the HER at room temperature for Pt/C plotted against the HBE for Pt(110) at the same pH. Values for $i_{0\text{-HER}}$ are from Zheng et al.[3], and the variation of HBE with pH from Sheng et al.[1] The top axis shows the pH values used to measure these reaction rates and HBEs.

The ln(TOF) of phenol hydrogenation and ln(i_0) are also plotted against the HBE to Pt(110) in Figure S3, where $i_{0\text{-HER}}$ is the electrochemical hydrogen evolution/oxidation reaction (HER/HOR) rate, using the exchange current density at 25 °C reported by Zheng et al.[3] The rate of phenol hydrogenation and electrochemical HER/HOR appear to change similarly with HBE (and pH), although the ln(i_0) increases with pH and HBE somewhat more rapidly at low acidity. The ln(i_0) dependence on HBE may change with temperature (i.e. at 80 °C rather than 25 °C as shown) if there is any change in activation barrier with HBE (or pH).

Catalytic hydrogenation of phenol over rhodium

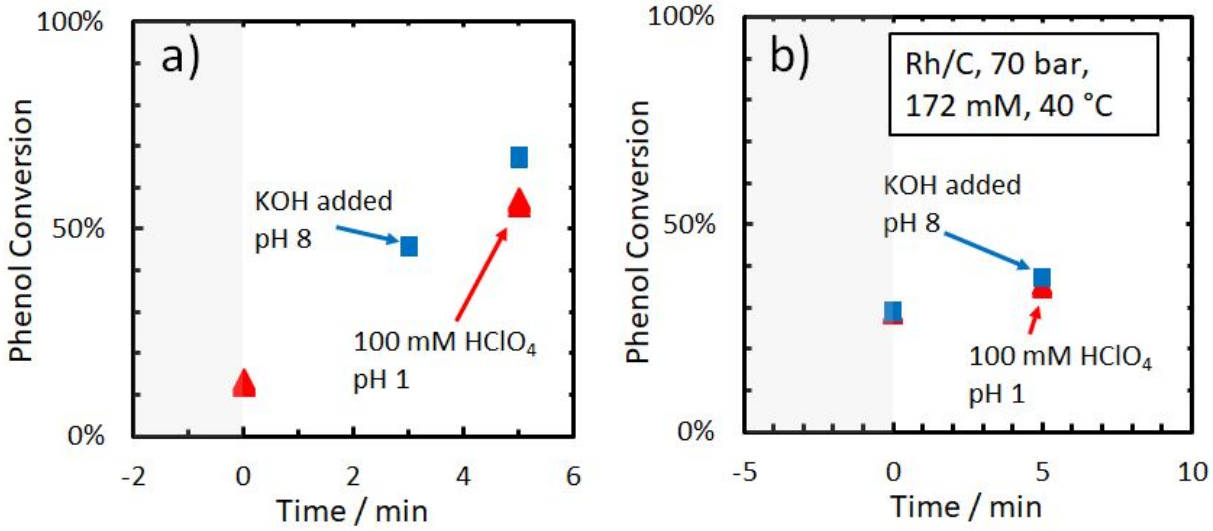

Figure S4. Conversion vs. time for Rh/C at different pH for hydrogenation of phenol (172 mM) in aqueous solution at a) 20 bar H_2 and 80 °C, b) 70 bar H_2 and 40 °C. Conversion at zero minutes is not-zero due to reaction during heat-up to 80 °C.

The conversion of phenol with respect to time is similar at pH 1 and pH 8 over a Rh/C catalyst, at 20 bar and 80 °C (Figure S4a) and 70 bar and 40 °C (Figure S4b). This behavior is different than what is observed for Pt/C, where at 20 bar hydrogen, there was a large increase in the TOF at pH 1 compared to pH 8.

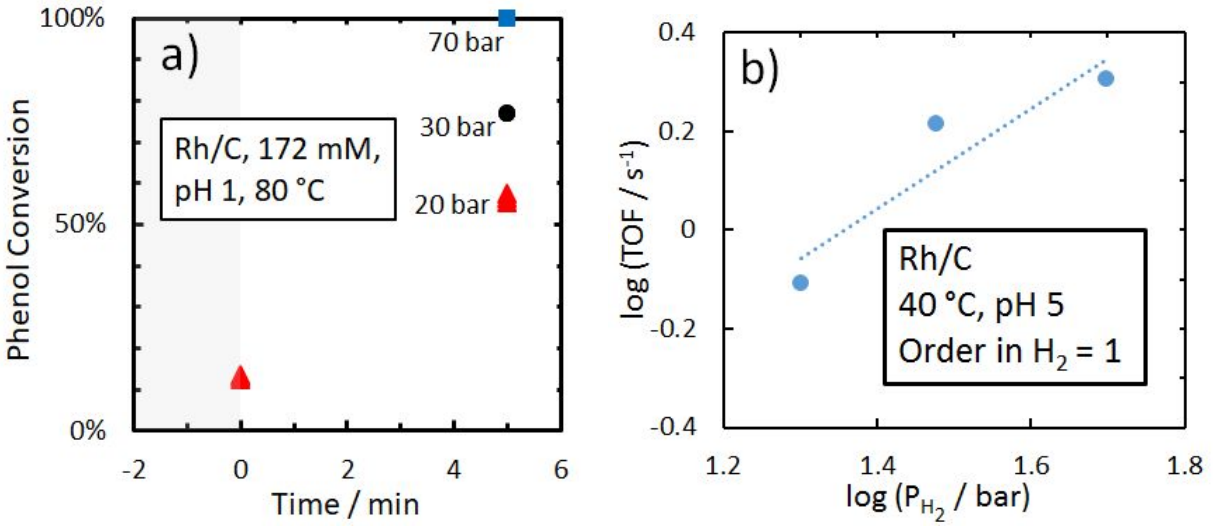

Figure S5. a) Conversion for phenol hydrogenation vs. time over 5 wt% Rh/C at pH 1 and 80 °C at different hydrogen pressures. b) Turnover frequencies for phenol hydrogenation as a function of pressure over 5 wt% Rh/C. Measurements at 40 °C and pH 5. Starting concentration of phenol was 172 mM. Conversion is non-zero at zero minutes due to conversion during heat-up to reaction temperature.

Increasing the hydrogen pressure increased the rate of phenol hydrogenation on Rh/C at 80 °C pH 1 and 40 °C pH 5 as shown in Figure 5. The hydrogen pressure dependence of phenol hydrogenation on Rh/C at 40 °C is near 1st order from 20 to 50 bar as shown in Figure S5b. The order in H_2 was measured at 40 °C due to the high rate of conversion at 80 °C (Figure 5a), which made initial rates difficult to obtain. This high positive order in H_2 is unlike what has previously been observed for Pt/C under these pressures (zero-order).[2]

Rate equations at high hydrogen coverages with changing hydrogen binding energy

In this section, we develop a reaction rate model assuming that the hydrogenation is zero-order in H_2 pressure based on a Langmuir adsorption. This means hydrogen coverage is not significantly changed by the hydrogen binding energy, which is related to K_{eq}^{H} (adsorption coefficient of H adatom).

By substituting Equation 2 into Equation 3 we get Equation S1:

$$E_a = \alpha + \beta\left(\Delta H^0_{f,Ph-H} - \Delta H^0_{f,Ph}\right) - \beta \times HBE \qquad \text{S1}$$

For an activated process that follows an Arrhenius relation, the TOF is given by Equation S2:

$$TOF = Aexp\left(\frac{-E_a}{RT}\right) \qquad \text{S2}$$

Assuming $\Delta H^0_{f,Ph-H} - \Delta H^0_{f,Ph}$ and surface coverages do not change with pH, Equations S1 and S2 can be combined to give Equation S3:

$$TOF = A'exp\left(\frac{\beta \times HBE}{RT}\right) \qquad \text{S3}$$

where *A'* is a new constant, differing from *A*. Taking the natural log of both sides gives Equation 4 (in the main text):

$$\ln\left(TOF\right) = \ln\left(A'\right) + \beta\left(\frac{HBE}{RT}\right) \qquad 4$$

Rates at low hydrogen coverages with changing hydrogen binding energy

At low hydrogen coverages,

$$TOF = A\,exp\left(\frac{-E_a}{RT}\right) = B\theta_H\theta_{Ph}exp\left(\frac{-E_a}{RT}\right) \qquad \text{S4}$$

where Θ_H is the hydrogen coverage and Θ_{Ph} is the phenol coverage. Assuming again that the energy of adsorbed phenol and hydrogenated phenol are not changed (relative to one another) with pH, Equation S4 can be rewritten as:

$$TOF = B'\theta_H\theta_{Ph}exp\left(\frac{\beta \times HBE}{RT}\right) \qquad \text{S5}$$

The coverages based on Langmuir competitive adsorption[1] can be included to give:

$$TOF = B'\frac{K_{eq}^{H}P_{H_2}^{1/2} * K_{eq}^{Phenol}C_{Ph}}{\left(1 + K_{eq}^{H}P_{H_2}^{1/2} + K_{eq}^{Phenol}C_{Ph}\right)^2}exp\left(\frac{\beta \times HBE}{RT}\right) \qquad \text{S6}$$

where we have replaced the "H" concentration with $P_{H_2}^{1/2}$, thus assuming 2nd-order desorption of H_{ad}, where K_{eq}^{H} is the equilibrium constant for H* adsorption from ½ H_2. This is related to HBE by:

$$K_{eq}^{H} = Cexp\left(\frac{-HBE}{RT}\right) \qquad \text{S7}$$

where *C* is a constant. (Note that there are often cases where the coverage of dissociated diatomics is found to increase instead first-order in the pressure (as is simple to prove when the adsorbate forms islands), so the exponent on the H_2 pressure here may be unity instead, but this would not change the effect of HBE derived below.) Under such conditions where the H_2 order is positive (n = 1/2 or 1) and phenol order is zero, $K_{eq}^{Phenol}C_{Ph} >> K_{eq}^{H}P_{H_2}^{n}$, and Equation S6 and Equation S7 can be combined to give Equation S8:

$$TOF = C'exp\left(\frac{-HBE}{RT}\right)P_{H_2}^{n}exp\left(\frac{\beta \times HBE}{RT}\right) \qquad \text{S8}$$

where the factors associated with phenol coverage and other constants are grouped together into a new constant, *C'*. This can be rewritten as Equation 6 in the main text:

$$TOF = C'P_{H_2}^{n}exp\left(\frac{(\beta - 1)HBE}{RT}\right) \qquad 6$$

A simpler way to derive this is to bypass Equation S6 and just assume θ_{Ph} is a constant (unaffected by the HBE at low θ_H), and replace θ_H in Equation S5 with $K_{eq}^{H}P_{H_2}^{n}$ (thereby grouping the constant site-blocking effect of θ_{Ph} on θ_H into K_{eq}^{H}, specifically as part of the constant *C*). If the right side of Equation S7 is then substituted for K_{eq}^{H}, and θ_{Ph} is grouped it into the constant C', it gives Equation S8.

Hydrogen coverage during phenol thermal catalytic hydrogenation over rhodium vs. platinum.

At 20 bar H_2, the hydrogenation rate of phenol is first order in H_2 pressure over Rh (Figure S5b), unlike Pt where the rate is zero order, indicating the hydrogen coverage is low on Rh but high on Pt. As a low hydrogen coverage on Rh would cause the hydrogenation rate to be modeled by Equation 6 (rather than Equation 3). Thus, the low hydrogen coverage on Rh under all pressures explains the independence of hydrogenation rate on pH (and HBE) for Rh using the same BEP

relationship as used for Pt. The lower coverage of hydrogen on Rh than on Pt under similar conditions in this work is somewhat expected, as Rh has a weaker hydrogen binding energy than Pt measured by TPD in gas-phase[4] and measured electrochemically under all pH values (with a difference of ~1-2 kJ/mol)[1]. In addition to the weaker HBE on Rh, calculations indicate stronger adsorption of the hydrocarbons on Rh than Pt (as calculated for phenol[5] and for benzene[6–8]), which inhibits buildup of a high coverage of hydrogen on Rh at 20 bar H_2 (and even up to 70 bar at 40 °C) if hydrogen and phenol compete for sites. As mentioned in the main text, Pd, which has a HBE greater than Pt[4], would be expected to behave similarly to Pt (high hydrogen coverage at pressures ~10 bar), with potential pH-dependence on rate. Ir, which has a HBE even weaker than Rh[4], would behave more similarly to Rh.

Computational details for the effect of pH on hydrogen binding energy on Pt(110)

Table S2. Computed time-averaged concentration (in mol/L) of hydronium ions H_3O^+, hydroxide ions OH^- and water from AIMD simulations of acidic, neutral and basic solution. Ion concentration was computed by calculating the coordination of oxygen atoms (3 = H_3O^+, 2 = H_2O and 1 = OH^-, using a cutoff distance d_{O-H} of 1.2 Å) averaged over all frames of the AIMD NVT trajectory after equilibration.

	acidic	neutral	alkaline
[H_3O^+]	1.4	0.0	0.0
[OH^-]	0.0	0.0	1.6
[H_2O]	45.4	46.8	46.7
Computed pH	0	7	14

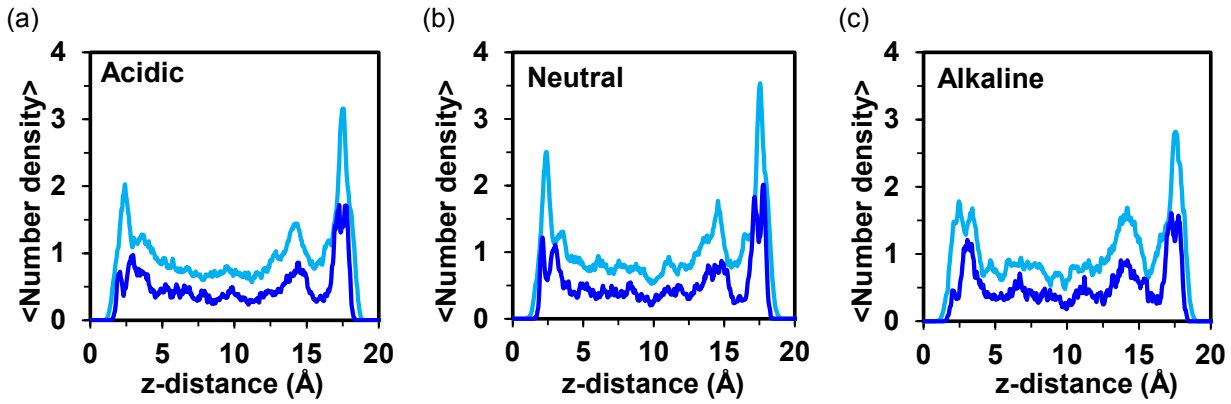

Figure S6. Atomic density profiles showing distribution of water oxygens O_{water} (**solid blue**) and water hydrogens H_{water} (**icy blue**) as a function of the Pt (110) surface normal direction (z) in (a) acidic (pH = 0), (b) neutral (pH = 7) and, (c) basic (pH = 14) solutions. z=0 denotes the metal surface. Values were obtained using average atomic distributions over the surface from all frames of the AIMD trajectory after equilibration.

Figure S6 shows the calculated disruption of the water molecules in acidic and alkaline conditions due to the presence of ions in the double layer. The pH also affects the orientation of the water dipoles in the solvent layer (Figure S7), which is attributed to the ions present in the double layer. Figure S8 shows the charge density distribution for acidic and alkaline conditions, and indicates the ions in the double layer cause the change in the electrostatic potential energy drop across the interfacial region ($\Delta\varphi$), explaining the results in Table 1.

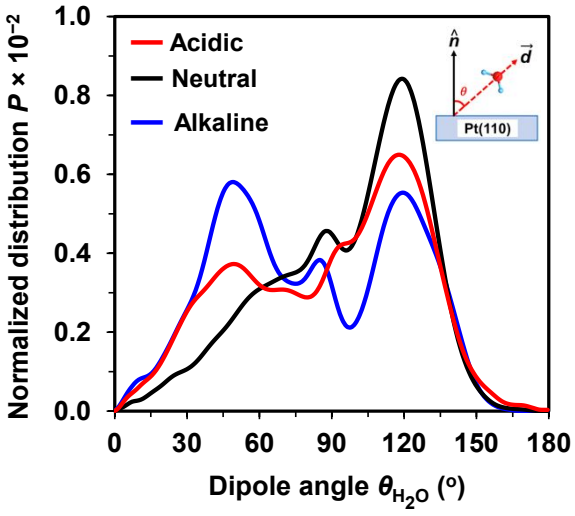

Figure S7. Average orientation (θ_{H_2O} in degrees) of the interfacial water dipoles (first solvent layer $0 < z < 2.6$ Å) relative to the Pt (110) surface in acidic (pH = 0), neutral (pH = 7) and alkaline (pH = 14) solutions. Values were obtained using dipole angle distributions averaged over all frames of the AIMD NVT trajectory.

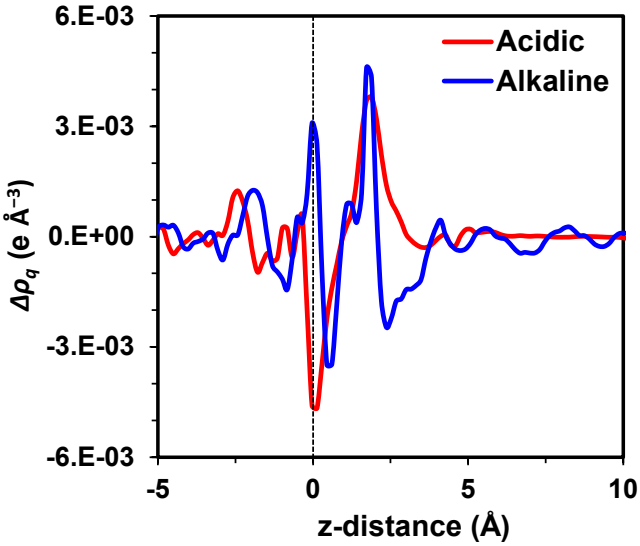

Figure S8. Differential charge density distribution ($\Delta\rho_q = \rho_{Total} - \rho_{Total-Ions} - \rho_{Ions}$) in the interfacial region in acidic (pH = 0) and alkaline (pH = 14) solutions. Positive values reflect electron gain and negative values reflect electron loss. Values were obtained from post-NVT annealed optimized strucutres. z=0 denotes the metal surface.

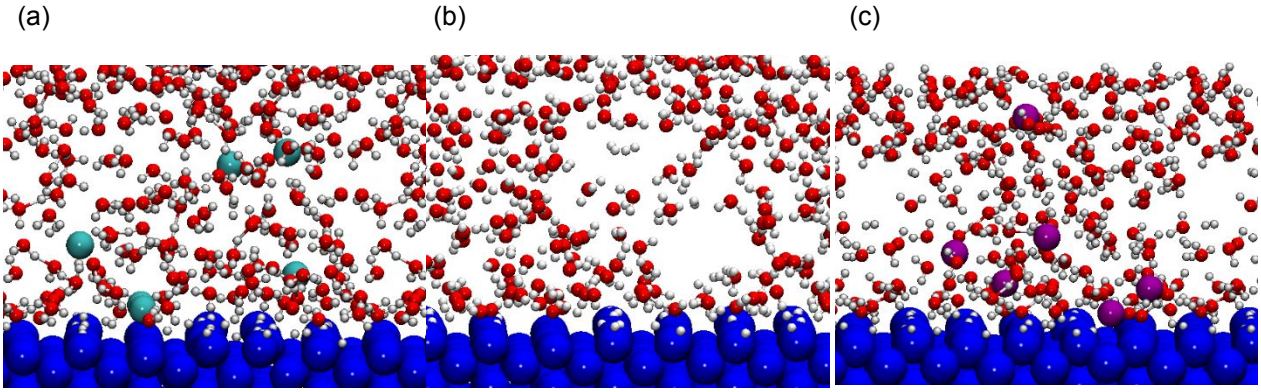

Figure S9. Simulation models of the solvated Pt (110) surface containing dissolved H_2 in (a) HCl solution (pH = 0), (b) H_2O (pH = 7) and, (c) NaOH solution (pH = 14). AIMD simulations were conducted within an NVT ensemble at 373 K. Atom color representations: Pt (**blue**), O (**red**), H (**silver**), Cl^- (**cyan**) and Na^+ (**purple**).

References

(1) Sheng, W.; Zhuang, Z.; Gao, M.; Zheng, J.; Chen, J. G.; Yan, Y. Correlating Hydrogen Oxidation and Evolution Activity on Platinum at Different pH with Measured Hydrogen Binding Energy. *Nat. Commun.* **2015**, *6*, 5848.

(2) Singh, N.; Song, Y.; Gutiérrez, O. Y.; Camaioni, D. M.; Campbell, C. T.; Lercher, J. A. Electrocatalytic Hydrogenation of Phenol over Platinum and Rhodium: Unexpected Temperature Effects Resolved. *ACS Catal.* **2016**, *6*, 7466–7470.

(3) Zheng, J.; Sheng, W.; Zhuang, Z.; Xu, B.; Yan, Y. Universal Dependence of Hydrogen Oxidation and Evolution Reaction Activity of Platinum-Group Metals on pH and Hydrogen Binding Energy. *Sci. Adv.* **2016**, *2*, 1–8.

(4) Silbaugh, T. L.; Campbell, C. T. Energies of Formation Reactions Measured for Adsorbates on Late Transition Metal Surfaces. *J. Phys. Chem. C* **2016**, *120*, 25161–25172.

(5) Honkela, M. L.; Björk, J.; Persson, M. Computational Study of the Adsorption and Dissociation of Phenol on Pt and Rh Surfaces. *Phys. Chem. Chem. Phys.* **2012**, *14*, 5849.

(6) Morin, C.; Simon, D.; Sautet, P. Chemisorption of Benzene on Pt(111), Pd(111), and Rh(111) Metal Surfaces : A Structural and Vibrational Comparison from First Principles. *J. Phys. Chem. B* **2004**, *108*, 5653–5665.

(7) Liu, W.; Carrasco, J.; Santra, B.; Michaelides, A.; Scheffler, M.; Tkatchenko, A. Benzene Adsorbed on Metals: Concerted Effect of Covalency and van Der Waals Bonding. *Phys. Rev. B - Condens. Matter Mater. Phys.* **2012**, *86*, 1–6.

(8) Carrasco, J.; Liu, W.; Michaelides, A.; Tkatchenko, A. Insight into the Description of van Der Waals Forces for Benzene Adsorption on Transition Metal (111) Surfaces. *J. Chem. Phys.* **2014**, *140*, 084704.